Stability analysis of perturbed plane Couette flow

Dwight Barkley
Mathematics Institute, University of Warwick, Coventry CV4 7AL, United Kingdom

Laurette S. Tuckerman
LIMSI-CNRS, BP 133, 91403 Orsay Cedex, France

(Received 16 December 1997; accepted 5 January 1999)

Plane Couette flow perturbed by a spanwise oriented ribbon, similar to a configuration investigated experimentally at the Centre d'Etudes de Saclay, is investigated numerically using a spectral-element code. Two-dimensional (2-D) steady states are computed for the perturbed configuration; these differ from the unperturbed flows mainly by a region of counter-circulation surrounding the ribbon. The 2-D steady flow loses stability to three-dimensional (3-D) eigenmodes at $\mathrm{Re}_c=230$, $\beta_c=1.3$ for $\rho=0.086$ and $\mathrm{Re}_c\approx 550$, $\beta_c\approx 1.5$ for $\rho=0.043$, where β is the spanwise wave number and 2ρ is the height of the ribbon. For $\rho=0.086$, the bifurcation is determined to be subcritical by calculating the cubic term in the normal form equation from the time series of a single nonlinear simulation; steady 3-D flows are found for Re as low as 200. The critical eigenmode and nonlinear 3-D states contain streamwise vortices localized near the ribbon, whose streamwise extent increases with Re. All of these results agree well with experimental observations. © *1999 American Institute of Physics.* [S1070-6631(99)00305-0]

I. INTRODUCTION

It is well known that, of the three shear flows most commonly used to model transition to turbulence, plane Poiseuille flow is linearly unstable for $\mathrm{Re}>5772$, whereas pipe Poiseuille flow and plane Couette flow are linearly stable for all Reynolds numbers; see, e.g., Ref. 1. Yet, as is also well established, in laboratory experiments, plane and pipe Poiseuille flows actually undergo transition to three-dimensional (3-D) turbulence for Reynolds numbers on the order of 1000. For plane Couette flow, the lowest Reynolds numbers at which turbulence can be produced and sustained has been shown to be between 300 and 400 both in numerical simulations[2,3] and in experiments.[4,5]

The gap between steady, linearly stable flows which depend on only one spatial coordinate and three-dimensional turbulence can be bridged by studying perturbed versions of Couette and Poiseuille flow. Plane Couette flow perturbed by a wire midway between the bounding plates and oriented in the spanwise direction has been the subject of laboratory experiments by Dauchot and co-workers[6–8] at CEA-Saclay. Our goal in this paper is to study numerically the flows and transitions in a configuration similar to that of the Saclay experiments.

Previous studies of plane channel flows have used a variety of approaches. We briefly review these, emphasizing computational investigations and the plane Couette case.

One approach is to seek finite amplitude solutions at transition Reynolds numbers and to understand the dynamics of transition in terms of these solutions. Finite amplitude solutions for plane Couette flow have been found for Reynolds numbers as low as $\mathrm{Re}=125$ by numerically continuing steady states or traveling waves from other flows: the wavy Taylor vortices of cylindrical Taylor–Couette flow by Nagata[9,10] and Conley and Keller,[11] and the wavy rolls of Rayleigh–Bénard convection by Busse.[12] Most recently, Cherhabili and Ehrenstein[13,14] succeeded in continuing plane-Poiseuille-flow solutions to plane Couette flow, via an intermediate Poiseuille–Couette family of flows. They showed that in proceeding from Poiseuille to Couette flow, the wave speed of the traveling waves decreases and their streamwise wavelength increases, as does the number of harmonics needed to capture them. When the Couette limit is reached, the finite amplitude solutions are highly streamwise-localized steady states. The minimum Reynolds number achieved in these continuations is $\mathrm{Re}=1500$. None of these steady solutions of plane Couette flow obtained so far are stable.

A second, highly successful, approach has been to study the transient evolution of linearized plane Couette flow. Although all initial conditions must eventually decay and the most slowly decaying mode must be spanwise invariant by Squire's theorem, the non-normality of the evolution operator allows large transient growth. Butler and Farrell[15] showed that a 1000-fold growth in energy could be achieved from an initial condition resembling streamwise vortices which are approximately circular and streamwise invariant. Reddy and Henningson[16] computed the maximum achievable growth for a large range of Reynolds numbers. An interpretation is given by these authors and by Trefethen *et al.*[17] in terms of pseudospectra: the spectra of non-normal operators display an extreme sensitivity to perturbations of the operator. Thus, slightly perturbed plane Couette or Poiseuille flows may be linearly unstable for much lower Reynolds numbers than the unperturbed versions.

A third broad category of computational investigation is the study of nonlinear temporal evolution in relatively tame turbulent plane channel flows. Orszag and Kells[18] and

Orszag and Patera[19] showed that finite amplitude spanwise-invariant states of plane Poiseuille flow are unstable to 3-D perturbations; this is also true of quasiequilibria for plane Poiseuille and Couette flow. Lundbladh and Johansson[2] showed that turbulent spots evolved from initial disturbances resembling streamwise vortices if the Reynolds number exceeded a critical Reynolds number between 350 and 375. Numerical simulations by Hamilton, Kim, and Waleffe[3] of turbulent plane Couette flow at Re=400 indicated that streamwise vortices and streaks played an important role in a quasicyclic regeneration process. Coughlin[20] used weak forcing to stabilize steady states containing streamwise vortices and streaks. These became unstable and underwent a similar regeneration cycle when the forcing or Reynolds number was increased. The critical Reynolds numbers displayed in all of these numerical simulations are in good agreement with experiments by Tillmark and Alfredsson[4] and by Daviaud *et al.*,[5] who reported turbulence at Re$\gtrsim$360 and Re $\gtrsim$370, respectively.

The last approach we discuss, and the most relevant to this study, is perturbation of the basic shear profile, to elicit instabilities that are in some sense nearby. If a geometric perturbation breaks either the streamwise or spanwise invariance of the basic profile, then the flow is freed from the constraint of Squire's theorem, which would otherwise imply that the linear instability at lowest Reynolds number is to a spanwise invariant two-dimensional (2-D) eigenmode. A perturbed flow with broken symmetry may directly undergo a 3-D linear instability. One can hope to understand the behavior of the unperturbed system by considering the limit in which the perturbation goes to zero. For some time, experimentalists[21] have used perturbations to produce spanwise-invariant Tollmien–Schlichting waves arising subcritically. More recently, for example, Schatz *et al.*[22] inserted a periodic array of cylinders in a plane Poiseuille experiment to render this bifurcation supercritical. In plane Couette flow, Dauchot and co-workers at Saclay[6–8] found that streamwise vortices could be induced for Reynolds numbers around 200 when a wire was placed in the flow (the exact range in Reynolds number for which the vortices occur depends on the radius of the wire). They suspected that these vortices arise from a subcritical bifurcation from the perturbed profile, but did not determine this.

In this paper, we numerically study the destabilization of plane Couette flow when a ribbon is placed midway in the channel gap (Fig. 1). The ribbon is infinitely thin in the streamwise (x) direction, occupies a fraction ρ of the cross-channel (y) direction, and is infinite in the spanwise (z) direction. This geometry is similar, though not identical, to that used in the Saclay experiments. In the experiments, the perturbation is a thin wire with cylindrical cross section. Here we use a ribbon because it is much easier to simulate numerically. For the experimental or numerical results to be of wider importance, the particular shape of the perturbation should not be important, as long as it is small.

We shall address the extent to which a small geometric perturbation of the plane Couette geometry affects the stability of the flow. We will show that a small geometric perturbation does indeed lead to a subcritical bifurcation to streamwise vortices, at Reynolds numbers and wave numbers which agree well with the Saclay experiments.

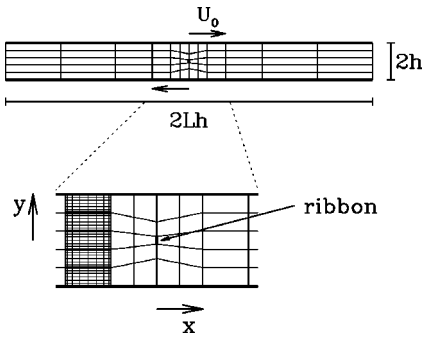

FIG. 1. Flow geometry considered in the paper. The upper and lower channel walls are separated by distance $2h$ and move with velocities $U_0\hat{x}$ and $-U_0\hat{x}$, respectively. An infinitely thin ribbon (the bold line) is located midgap in the channel and has height $2\rho h$ ($\rho=0.086$ for the case shown). The computational mesh (macro elements) used in our calculations is shown, as is the (fine) collocation mesh for polynomial order $N=8$ (five elements in the enlargement). The ribbon is formed by setting no-slip boundary conditions on the edges of two adjoining elements. Periodic boundary conditions are imposed over length $2Lh$ in the horizontal direction. The full geometry shown has aspect ratio $L=10$. The system is homogeneous in the spanwise (z) direction normal to the figure.

II. NUMERICAL COMPUTATIONS

The computations consist of three parts: (1) obtaining steady 2-D solutions of the Navier–Stokes equations, (2) determining the linear stability of these solutions to 3-D perturbations, and (3) classifying the bifurcation via a nonlinear stability analysis. Here we outline the numerical techniques for carrying out these computations.

A. 2-D steady flows

Our computational domain has been shown in Fig. 1. We nondimensionalize lengths by the channel half-height h, velocities by the speed U_0 of the upper channel wall, time by the convective time h/U_0. There are two nondimensional parameters for the flow, which we take to be the usual Reynolds number for plane Couette flow, $\mathrm{Re}=hU_0/\nu$, where ν is the kinematic viscosity of the fluid, and the nondimensional half-height of the ribbon ρ, hereafter called its radius for consistency with the Saclay experiments. We view the (nondimensionalized) streamwise periodicity length $2L$ as a numerical parameter which we take sufficiently large that the system behaves as though it were infinite in the streamwise direction.

The fluid flow is governed by the incompressible Navier–Stokes equations:

$$\frac{\partial \mathbf{u}}{\partial t} = -(\mathbf{u}\cdot\boldsymbol{\nabla})\mathbf{u} - \boldsymbol{\nabla} p + \frac{1}{\mathrm{Re}}\nabla^2\mathbf{u} \quad \text{in } \Omega, \tag{1a}$$

$$\boldsymbol{\nabla}\cdot\mathbf{u} = 0 \quad \text{in } \Omega, \tag{1b}$$

subject to the boundary conditions:

$$\mathbf{u}(x-L,y) = \mathbf{u}(x+L,y), \tag{2a}$$

$$\mathbf{u}(x,y=\pm 1) = \pm\hat{\mathbf{x}}, \tag{2b}$$

$$\mathbf{u}(x=0,y)=0 \quad \text{for } -\rho\leqslant y\leqslant\rho, \tag{2c}$$

where $\mathbf{u}\equiv(u,v,w)$ is the velocity field, p is the nondimensionalized static pressure, and Ω is the computational domain. The pressure p, like $\mathbf{u}$, satisfies periodic boundary conditions in x.

Time-dependent simulations of these equations in two dimensions ($w\equiv 0$, $\partial/\partial z\equiv 0$) are carried out using the spectral element[23] program PRISM.[24,25] In the spectral element method, the domain is represented by a mesh of macroelements as shown in Fig. 1. The channel height is spanned by 5 elements while the number of elements spanning the streamwise direction depends on its length: 24 elements are used for $L=32$ and 36 elements for $L=56$. The no-slip condition (2c) is enforced by setting zero velocity boundary conditions along the edges of two adjoining mesh elements: This interface defines the ribbon. If continuity were imposed along this interface, as is done on all other element boundaries, then the flow would reduce to unperturbed plane Couette flow. Thus the ribbon is modeled by a small (but significant) change in the boundary conditions on just two edges of elements in the computational domain. Within each element both the geometry and the solution variables (velocity and pressure) are represented using Nth order tensor-product polynomial expansions. The collocation mesh in Fig. 1 (enlargement) corresponds to an expansion with $N=8$.

A time-splitting scheme is used to integrate the underlying discretized equations.[26] Based on simulations with polynomial order N in the range $6\leqslant N\leqslant 12$ and time steps Δt in the range $10^{-3}\leqslant\Delta t\leqslant 10^{-2}$ we have determined that $N=8$ and $\Delta t=0.005$ give valid results over the range of Re considered. These numerical parameter values (typical for studies of this type) have been used for most of the results reported. Each velocity component is thus represented by about 7500 scalars for $L=32$.

Steady flows used for our stability calculations have been obtained from simulations with Reynolds numbers in the range $100\leqslant \mathrm{Re}\leqslant 600$. In all cases, the simulations were run sufficiently long to obtain asymptotic, steady velocity fields. We shall denote these steady 2-D flows by $\mathbf{U}(x,y)$.

B. Linear stability analysis

Let $\mathbf{U}(x,y)$ be the 2-D base flow whose stability is sought. An infinitesimal three-dimensional perturbation $\mathbf{u}'(x,y,z,t)$ evolves according to the Navier–Stokes equations linearized about $\mathbf{U}$. Because the resulting linear system is homogeneous in the spanwise direction z, generic perturbations can be decomposed into Fourier modes with spanwise wave numbers β:

$$\begin{aligned}\mathbf{u}'(x,y,z,t)&=(\hat{u}\cos\beta z,\hat{v}\cos\beta z,\hat{w}\sin\beta z),\\ p'(x,y,z,t)&=\hat{p}\cos\beta z\end{aligned} \tag{3}$$

or an equivalent form obtained by translation in z. The vector $\hat{\mathbf{u}}(x,y,t)=(\hat{u},\hat{v},\hat{w})$ of Fourier coefficients evolves according to:

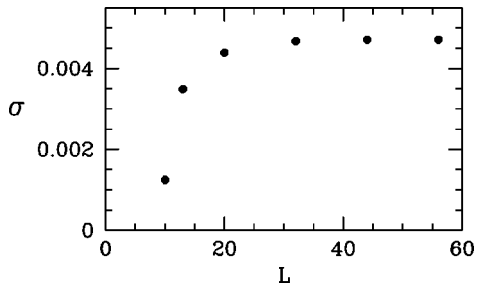

FIG. 2. Leading eigenvalue as a function of streamwise periodicity half-length L for Re=250, $\beta=1.3$. For $L\gtrsim 32$ the eigenvalue is independent of L.

$$\frac{\partial\hat{\mathbf{u}}}{\partial t}=-(\hat{\mathbf{u}}\cdot\boldsymbol{\nabla})\mathbf{U}-(\mathbf{U}\cdot\boldsymbol{\nabla})\hat{\mathbf{u}}-(\boldsymbol{\nabla}-\beta\hat{\mathbf{z}})\hat{p}+\frac{1}{\mathrm{Re}}(\nabla^2-\beta^2)\hat{\mathbf{u}} \quad \text{in } \Omega, \tag{4a}$$

$$(\boldsymbol{\nabla}+\beta\hat{\mathbf{z}})\cdot\hat{\mathbf{u}}=0 \quad \text{in } \Omega, \tag{4b}$$

where $\boldsymbol{\nabla}$, etc., are two-dimensional differential operators. Equation (4) is solved subject to homogeneous boundary conditions:

$$\hat{\mathbf{u}}(x-L,y)=\hat{\mathbf{u}}(x+L,y), \tag{5a}$$

$$\hat{\mathbf{u}}(x,y=\pm 1)=0, \tag{5b}$$

$$\hat{\mathbf{u}}(x=0,y)=0 \quad \text{for } -\rho\leqslant y\leqslant\rho. \tag{5c}$$

Equation (4) with boundary conditions (5) can be integrated numerically by the method described in Sec. II A. For fixed β, this is essentially a two-dimensional calculation.[27,28] After integrating (4)–(5) a sufficiently long time, only eigenmodes corresponding to leading eigenvalues remain. We use this to find the leading eigenvalues (those with largest real part) and corresponding eigenmodes for fixed values of Re and β as follows. A Krylov space is constructed based on integrating (4)–(5) over $K=8$ successive (dimensionless) time intervals of $T=5$. More precisely, we calculate the fields $\hat{\mathbf{u}}(t)$, $\hat{\mathbf{u}}(t+T),\ldots,\hat{\mathbf{u}}(t+(K-1)T)$ and orthonormalize these to form a basis $v_1,v_2,\ldots,v_K$. We then define the $K\times K$ matrix $H_{ij}\equiv\langle v_i,\mathbf{L}v_j\rangle$ where $\mathbf{L}$ is the operator on the right-hand side of the linearized Navier–Stokes equations and $\langle\,\rangle$ is an inner product. Approximate eigenvalues σ and eigenmodes $\tilde{\mathbf{u}}(x,y,z)$ are calculated by diagonalizing H and using (3) to reconstruct 3-D fields. Their accuracy is tested by computing the residual $r\equiv\|\sigma\tilde{\mathbf{u}}-\mathbf{L}\tilde{\mathbf{u}}\|$. If the eigenvalue–eigenmode pairs do not attain a desired accuracy ($r<10^{-5}$ for the case here), then another iteration is performed. The new vector is added to the Krylov space and the oldest vector is discarded. This is effectively subspace iteration initiated with a Krylov subspace. More details can be found in Refs. 22, 27, and 29.

We conclude this section by considering the effect of the streamwise periodicity length $2L$ on the computations. Recall that we view L as a quasinumerical parameter in that we seek solutions valid for large L. Figure 2 shows the dependence of the leading eigenvalue σ on streamwise length at Re=250, $\beta=1.3$ (values near the primary 3-D linear instability). It can be seen that for $L\gtrsim 32$ the eigenvalue is inde-

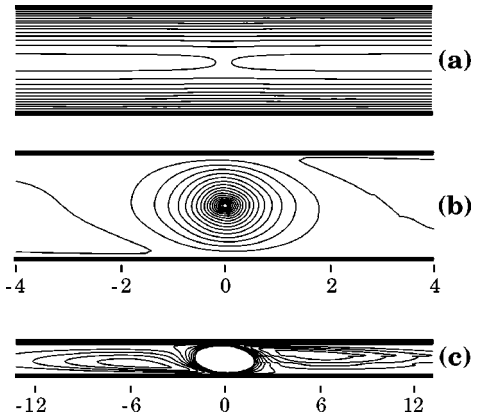

FIG. 3. The steady two-dimensional base flow $\mathbf{U}(x,y)$ at Re=250 for a ribbon with $\rho=0.086$. Only the central portion of the full $L=32$ domain is shown. (a) Streamfunction contours of $\mathbf{U}$. The flow is nearly identical to the parallel shear of plane Couette flow except very near the ribbon. (b) Streamfunction contours of the deviation $\mathbf{U}-\mathbf{U}_C$ highlighting the difference between the perturbed and unperturbed Couette flows. A region ($|x|\lesssim 3$) of positive circulation is established around the ribbon. The flow is centrosymmetric. (c) The deviation over a larger streamwise extent showing regions ($3\lesssim|x|\lesssim 24$) further from the ribbon whose circulation is negative, like that of $\mathbf{U}_C$. The flow is very weak; contours of the dominant part of this flow are not shown. The slight lack of centrosymmetry is a graphical artifact.

pendent of L. This is consistent with the structure of the base flow and eigenmodes shown in Sec. III. Most of the computations reported have used $L=32$.

C. 3-D simulations

For the nonlinear stability analysis and for obtaining steady 3-D flows, we carry out 3-D simulations of (1)–(2) using the same spectral element representation in (x,y) described above together with a Fourier representation in the spanwise direction z. We impose periodicity in the spanwise direction by including wave numbers $m\beta_c$ for integers $|m|<M/2$, where β_c is the critical wave number found in the linear stability analysis. The simulations we report use $M=16$.

III. RESULTS

A. 2-D steady flows

A typical steady 2-D flow for the perturbed Couette geometry is shown in Fig. 3. It is representative of base flows for Reynolds numbers on the order of a few hundred with a ribbon of size $\rho=0.086$. This was chosen to correspond to the radius of one of the cylinders used in the Saclay experiments.[6–8] The Reynolds number Re=250 of the flow shown is close to the threshold for the 3-D instability that will be discussed in Sec. III B. Unless otherwise stated, results are for $\rho=0.086$, Re=250, and $L=32$.

In Fig. 3(a) it can been seen that, except near the ribbon, the steady flow is essentially the parallel shear of unperturbed plane Couette flow. The streamlines are as reported experimentally in Ref. 6. As noted there, the Reynolds number based on the radius of the ribbon and the local velocity near the ribbon is very small compared to Reynolds numbers where separation or vortex shedding could be expected. In Fig. 3(b) we plot the streamfunction of the deviation $\mathbf{U}-\mathbf{U}_C$ where $\mathbf{U}_C=y\hat{\mathbf{x}}$ is the unperturbed plane Couette profile. The primary effect of the ribbon is to establish a region ($|x|\lesssim 3$) of positive circulation (opposing that of plane Couette flow) surrounding the ribbon. Figure 3(c) shows $\mathbf{U}-\mathbf{U}_C$ over a larger streamwise extent. Further from the ribbon are wider regions ($3\lesssim|x|\lesssim 24$) in which the deviation is weak, but has the same negative circulation as plane Couette flow.

The size of the counter-rotating region is remarkably uniform over the ribbon radii and Reynolds numbers that we have studied. We define the streamwise extent of the counter-rotating region as delimited by $\psi(x,y=0)=0$, i.e., the x values at which the streamfunction at midheight $y=0$ has the same value as at the channel walls $y=\pm 1$. For $\rho=0.086$, the counter-rotating region varies from $|x|\leqslant 2.18$ for Re=150 to $|x|\leqslant 3.00$ for Re=300, while for $\rho=0.043$ the counter-rotating region varies from $|x|\leqslant 2.10$ for Re=150 to $|x|\leqslant 2.87$ for Re=600. This insensitivity to the size of ρ is significant in light of the 2-D finite-amplitude steady states calculated by Cherhabili and Ehrenstein.[13,14] The states found by these authors in unperturbed plane Couette flow strongly resemble that in Fig. 3. These too have a central counter-rotating region surrounded by larger regions of negative circulation. At Re=2200, the counter-rotating region in their flow occupies $|x|\leqslant 2.31$ (see Figs. 10 and 11 of Ref. 13, Figs. 2 and 3 of Ref. 14) The similarity between the 2-D flows for $\rho=0.086$, $\rho=0.043$, and, effectively, $\rho=0$ leads us to hypothesize that our 2-D perturbed plane Couette flows are connected (via the limit $\rho\to 0$) to those computed by Cherhabili and Ehrenstein.

We may also quantify the intensity of the counter-circulation. One measure is the maximum absolute value of v, which is attained very near the ribbon, at $(x,y)=(\pm 0.081,0)$. This value is approximately independent of Reynolds number, but decreases strongly with ribbon radius: $v_{\max}\approx 0.031$ for $\rho=0.086$ and $v_{\max}\approx 0.013$ for $\rho=0.043$.

An important qualitative feature of the flow can be seen in Figs. 3(b) and 3(c): The flow is centrosymmetric, i.e., it is invariant under combined reflection in x and y, or equivalently rotation by angle π about the origin. It can be verified that the governing equations (1) and boundary conditions (2) are preserved by the centrosymmetric transformation:

$$\mathbf{u}(x,y)\to -\mathbf{u}(-x,-y). \tag{6}$$

The unperturbed plane Couette problem is also centrosymmetric. It is in fact symmetric under the Euclidean group E_1 of translations and the ''reflection'' consisting of the centrosymmetric transformation (6). The ribbon in the perturbed flow breaks the translation symmetry, but leaves the centrosymmetry intact. Note that reflections in x or y alone are not symmetries of either the unperturbed or the perturbed plane Couette problem because either reflection alone reverses the direction of the channel walls, violating the boundary conditions (2b).

In Fig. 4 we present streamwise velocity profiles near the ribbon. For $|x|>0.5$, the Couette profile is very nearly recovered. Figure 4(b) shows streamwise velocity profiles of the deviation from the linear Couette profile across the full chan-

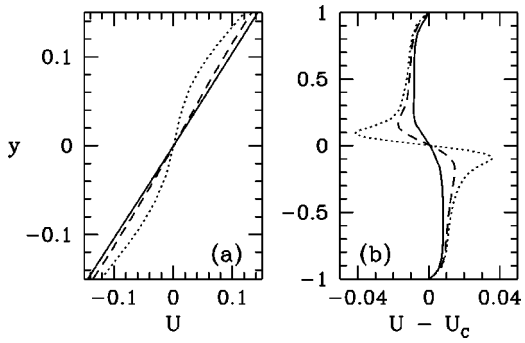

FIG. 4. Streamwise velocity profiles in the perturbed geometry. (a) $U(x,y)$ as a function of y for $x=0.081$ (dotted), $x=0.25$ (dashed), and $x=0.5$ (solid). Only the central portion of the channel is shown. Only very close to the ribbon does the velocity differ significantly from the linear profile. (b) Deviation $U(x,y)-y$ over the full range of y.

nel. Close examination reveals that these profiles are not odd in y, consistent with the fact that the system is neither symmetric nor antisymmetric under reflection in y. The symmetric partners to the profiles shown are at negative x values.

The profiles in Fig. 4 are similar to those Bottin *et al.*[8] obtained in the Saclay experiments under similar conditions. It is not possible to compare directly with experiment because of the difficulty in obtaining experimental velocity profiles and because the geometric perturbations differ in the computations and experiments. The only noticeable difference between experiments and computations is that the profiles Fig. 4(b) are very nearly odd in y, whereas in experiment this lack of symmetry is more pronounced.

Finally in Fig. 5 we quantify the deviation between perturbed and unperturbed plane Couette flow by plotting the energy per unit length $E(\mathbf{U}-\mathbf{U}_C)\equiv\int_{-1}^{1}dy\,\frac{1}{2}|\mathbf{U}(x,y)-\mathbf{U}_C(y)|^2$ as a function of x for $-56\leqslant x\leqslant 56$. The data show a narrow central region, corresponding to the region $|x|\leqslant 2.76$ of positive circulation seen in Fig. 3(b), where the deviation falls sharply and approximately exponentially in x. For $|x|>2.76$, the deviation, while very small, decays very slowly (and not exponentially) with $|x|$. The boundaries $x=\pm 23.78$ terminating the outer region of negative circulation can also be seen in Fig. 5. The precision of the computations is surpassed beyond $|x|=40$. Figure 5 shows that for $|x|>32$ the deviation of the base flow from Couette is indeed very weak and this supports our choice of $L=32$ as an adequate domain size for most computations.

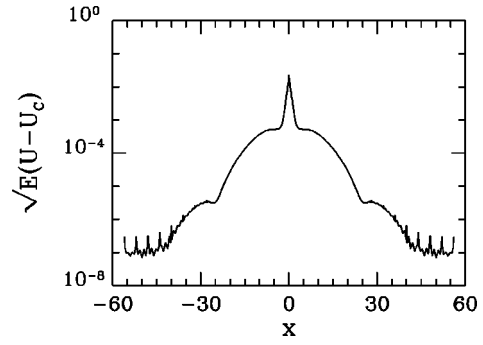

FIG. 5. Energy of deviation between perturbed and unperturbed Couette flows as a function of x. Parameters are the same as in Fig. 3 except that here $L=56$. Abrupt changes in slope at $|x|=2.76$, $|x|=23.78$ correspond to changes in the sign of the circulation of $\mathbf{U}-\mathbf{U}_C$. For $|x|\gtrsim 40$, the deviation is below the precision of the computations.

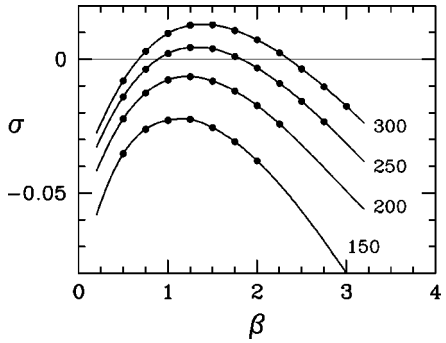

FIG. 6. Growth rate σ of most unstable three-dimensional eigenmode as a function of spanwise wave number β for Re=150,200,250,300 with ribbon radius $\rho=0.086$. Critical values for instability are $\mathrm{Re}_c=230$ and $\beta_c=1.3$.

B. 3-D linear stability results

The two-dimensional steady flows just discussed become linearly unstable to three-dimensional perturbations when the Reynolds number exceeds a critical value Re_c. To determine this value and the associated wave number, we have performed a linear stability analysis of the steady flows via the procedure described in Sec. II B.

Figure 6 shows the growth rate σ of the most unstable three-dimensional eigenmode $\hat{\mathbf{u}}$ as a function of Re and spanwise wave number β for a ribbon with $\rho=0.086$. For each value Re, we have fit a piecewise-cubic curve, shown in Fig. 6, through the eigenvalue data to determine the wave number $\beta_{\max}(\mathrm{Re})$ which maximizes σ. The critical Reynolds number Re_c is then determined by linear interpolation of $\sigma[\beta_{\max}(\mathrm{Re}),\mathrm{Re}]$ through these maxima and finding its zero crossing. From this we find critical values for the onset of linear instability to be $\mathrm{Re}_c=230$ and $\beta_c=1.3$ for the ribbon with $\rho=0.086$. These values are consistent with what is seen experimentally, but we delay discussion until the conclusion.

Figure 7 shows similar eigenvalue spectra for a ribbon half as large: $\rho=0.043$. The critical wave number $\beta_c\approx 1.5$ is only slightly larger than the previous value. However, the critical Reynolds number is much larger: $\mathrm{Re}_c\approx 550$. The

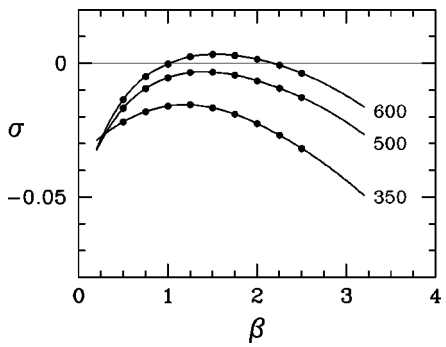

FIG. 7. Growth rate of the most unstable eigenmode as a function of β and Re for $\rho=0.043$. Critical values are $\mathrm{Re}_c\approx 550$ and $\beta_c\approx 1.5$.

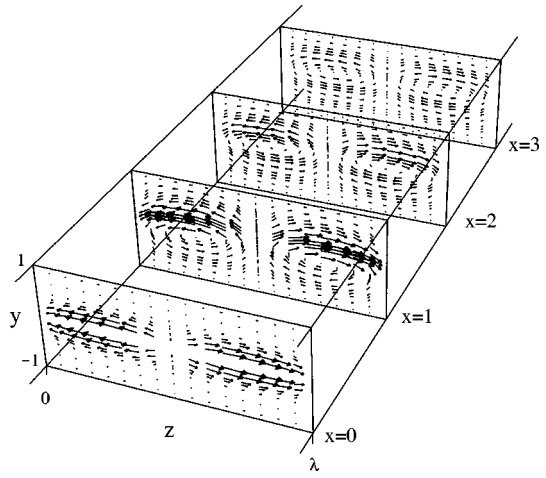

FIG. 8. Velocity field of near-marginal eigenvector in the planes $x=0$, $x=1$, $x=2$, and $x=3$. Parameters are Re=250, $\rho=0.086$, $L=32$, $\lambda=4.83$. At $x=0$, the velocity is reflection-symmetric in y and primarily spanwise. The ribbon is seen as the area $|y|<\rho=0.086$ with no flow. Streamwise vortices are visible for $x\geqslant 1$. The scale for distances in x is stretched by a factor of 3.333 relative to distances in y,z.

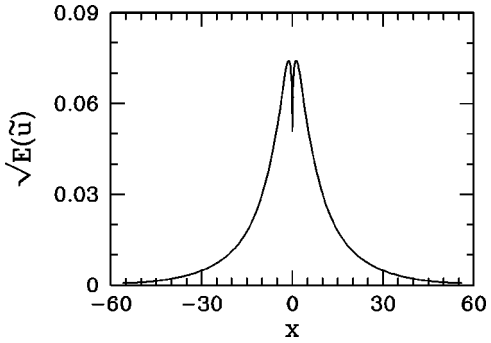

FIG. 10. Energy of near-marginal eigenvector as a function of x. Parameters are the same as in Figs. 8 and 9 except that here $L=56$. Vertical scale is arbitrary.

critical Reynolds number must increase as ρ is decreased since, when no ribbon is present, the problem reduces to classical plane Couette flow which is linearly stable for all finite Re, i.e., $\lim_{\rho\to 0}\mathrm{Re}_c(\rho)=\infty$.

We note that Cherhabili and Ehrenstein[14] also calculate 3-D instability for their 2-D finite amplitude plane Couette flows. Despite the resemblance of their 2-D flows to ours, the spanwise wave number corresponding to maximal growth is much larger in their case: $\beta\approx 23$.

A computed eigenvector $\tilde{\mathbf{u}}=(\tilde{u},\tilde{v},\tilde{w})$ is shown in Figs. 8 and 9. This eigenvector is near marginal: Re=250, close to $\mathrm{Re}_c=230$. The spanwise wavelength is $\lambda=\lambda_c\equiv 2\pi/\beta_c=4.83$. The other parameters are $\rho=0.086$ and $L=32$.

Figure 8 shows $(\tilde{v},\tilde{w})$ velocity plots at four streamwise locations. In the $x=0$ plane containing the ribbon, the flow is reflection symmetric in y, and the flow is primarily spanwise. The trigonometric dependence in z with the choice of phase (3) can be seen. In the planes $x=1$, $x=2$, and $x=3$, two counter-rotating streamwise vortices are present. The flow for negative x is obtained by reflection in y.

Figure 9 presents two complementary views of the eigenvector $\tilde{\mathbf{u}}$ for $-1<x<13$. Above is a plot of $(\tilde{u},\tilde{v})$ in the plane $z=0$ where they are maximal [cf. Eq. (3)]. Below is a plot of $(\tilde{u},\tilde{w})$ in the plane $y=0$ at midchannel height.

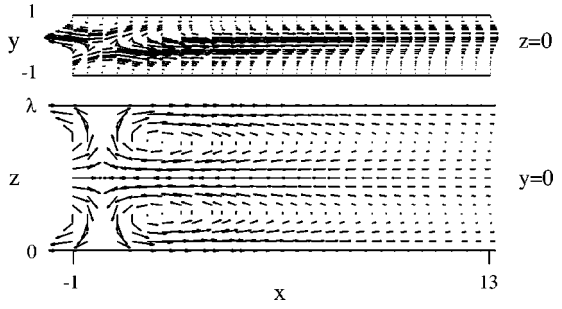

FIG. 9. Velocity field of near-marginal eigenvector in the planes $z=0$ and $y=0$.

Figure 10 shows the x dependence of the spanwise-averaged energy per unit length

$$E(\tilde{\mathbf{u}})\equiv\frac{1}{\lambda_c}\int_0^{\lambda_c}dz\int_{-1}^{+1}dy\,\frac{1}{2}|\tilde{\mathbf{u}}|^2. \tag{7}$$

Here, the eigenvector was computed in a larger domain ($L=56$) in order to determine its long-range behavior. The eigenvector is localized: the energy decays exponentially with $|x|$ and does not reflect the counter- and corotating regions of the 2-D base flow seen in Fig. 5. The flow deficit due to the ribbon produces the local minimum at $x=0$.

We have also computed the vorticity of the eigenvector. Despite the streamwise vortices visible in Fig. 8, ω_x is the smallest vorticity component and ω_z by far the largest over most of the domain.

C. 3-D nonlinear stability results

Our method of nonlinear stability analysis has previously been used to determine the nature of the bifurcation to three dimensionality in the cylinder wake.[28] The method is based on tracking the nonlinear evolution of the 3-D flow starting from an initial condition near the bifurcation at Re_c. ''Near'' refers both to phase space (i.e., a small 3-D perturbation from the two-dimensional profile) and to parameter space (i.e., at a Reynolds number slightly above the linear instability threshold). In essence we follow the dynamics along the unstable manifold of the 2-D steady flow far enough to determine how the nonlinear behavior deviates from linear evolution. From this we can determine very simply whether the instability is subcritical or supercritical.

Three-dimensional simulations are carried out for $\rho=0.086$ at Re=250, slightly above $\mathrm{Re}_c=230$, starting with an initial condition of the form:

$$\mathbf{u}(x,y,z)=\mathbf{U}(x,y)+\epsilon\tilde{\mathbf{u}}(x,y,z), \tag{8}$$

where $\mathbf{U}$ is the 2-D base flow at Re=250, $\tilde{\mathbf{u}}$ is its eigenmode at wave number $\beta_c=1.3$, and ϵ is a small number controlling the size of the initial perturbation.

The restriction to wave numbers which are multiples of β_c accurately captures the evolution from initial condition (8), since the Navier–Stokes equations preserve this sub-

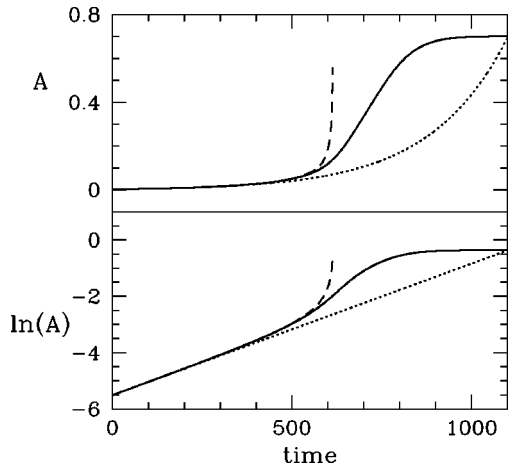

FIG. 11. Nonlinear growth of the amplitude A of the 3-D flow from simulation (solid) at Re=250 plotted on linear and logarithmic scales. First-order (dotted) and third-order (dashed) dynamics are shown with $\sigma=0.004\,669$ and $\alpha=0.9$. The faster than exponential nonlinear growth (i.e., positive α) shows that the instability at Re_c is subcritical.

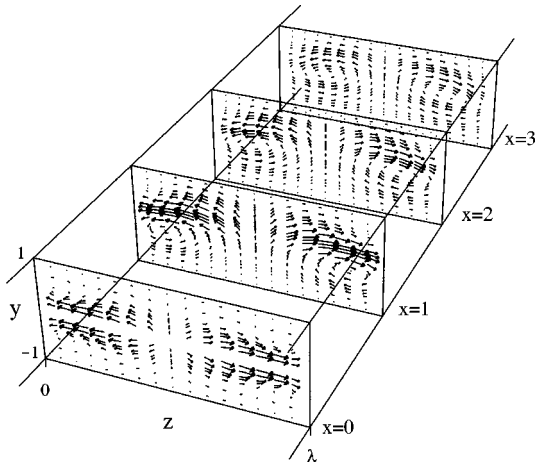

FIG. 12. 3-D velocity field in the planes $x=0$, $x=1$, $x=2$, and $x=3$. Parameters are Re=200, $\rho=0.086$, $L=32$, $\lambda=4.83$. At $x=0$, four small streamwise vortices can be seen in the corners of the domain. The lower ($y<0$) vortex pair evolves into the large vortices seen at $x=1$. The scale for distances in x is stretched by a factor of 3.333 relative to distances in y,z.

space of 3-D solutions. That is, we seek only to follow the evolution in the invariant subspace containing the critical eigenmode. We do not address the issue of whether the λ_c-periodic flow is itself unstable to long-wavelength perturbations.

To analyze the nonlinear evolution, we define the (real) amplitude A of the 3-D flow as

$$A\equiv\left[\frac{1}{\lambda_c}\int_0^{\lambda_c}dz\int_{-1}^{+1}dy\int_{-L}^{+L}dx\,\frac{1}{2}|\mathbf{u}_1|^2\right]^{1/2}, \tag{9}$$

where $\mathbf{u}_1(x,y,z,t)$ is the component of the 3-D velocity field at wave number β_c, i.e., A is the square root of the energy of the flow at wave number β_c. (A complex amplitude, not required here, would include the phase of the solution in the spanwise direction.)

Figure 11 shows the time evolution of A from our simulations. The value of ϵ is such that the initial energy of the 3-D perturbation, $\epsilon\tilde{\mathbf{u}}$, is $E=A^2=1.66\times10^{-5}$; the energy of the base flow $\mathbf{U}$ is $E=21.3$.

To interpret the nonlinear evolution, consider the normal form for a pitchfork bifurcation including terms up to third order in the amplitude:

$$\dot{A}=\sigma A+\alpha A^3. \tag{10}$$

The leading nonlinear term is cubic because the 3-D bifurcation is of pitchfork type [an $O(2)$ symmetric pitchfork bifurcation]. The Landau coefficient α determines the nonlinear character of the bifurcation. If $\alpha>0$, then the nonlinearity is destabilizing at lowest order and the bifurcation is subcritical; if $\alpha<0$, then the cubic term saturates the instability and the bifurcation is supercritical.

Figure 11 includes curves for first-order evolution (i.e., $\dot{A}=\sigma A$) and the third-order evolution given by Eq. (10). For the first-order evolution, the eigenvalue σ for the bifurcation has been computed via the linear stability analysis in Sec. III B. For the third-order evolution we have simply fit the one remaining parameter, α, in the normal form. We followed the approach in Ref. 28 of using the time series $A(t)$ and the known value of σ to estimate α from $\alpha\simeq(\dot{A}-\sigma A)/A^3$. This gives $\alpha=0.9\pm0.05$, a constant value for $T\leqslant500$, which determines how long the third-order truncation is valid in this case. The value of α is essentially unchanged when the mesh is refined by increasing the polynomial order N to 10 or the number M of Fourier modes to 32. The magnitude of α depends on the definition of A, but its sign does not. The fact that α is positive indicates that the instability is subcritical. Figure 11 indicates that the 3-D flow has become steady by $t\approx1000$. The nonlinear saturation seen in the time series is not captured by including a fifth-order term in the normal form.

We have verified that the instability is subcritical by computing nonlinear states below Re_c. In Fig. 12, we show the steady 3-D flow at Re=200. Figure 12 is analogous to Fig. 8 depicting the eigenvector, so we will emphasize here the ways in which the two flows differ. Small streamwise vortices can be seen in each of the four corners of the $x=0$ plane containing the ribbon. The lower ($y<0$) pair evolve with x into the strong pair of vortices at $x=1$. The vortices at $x=3$ are tilted with respect to their counterparts in the eigenvector, attesting to the nonlinear generation of the second spanwise harmonic 2β. The 3-D flow in the $y=0$ and $z=0$ planes (after subtraction of the dominant 2-D base flow) is sufficiently similar to the eigenvector (Fig. 9) that we do not present it here.

Streamwise velocity u contours of the 3-D flow at $x=2$ are shown in Fig. 13. The (v,w) projections of our 3-D flow in Fig. 12, showing the tilted streamwise vortices, resemble the depictions of optimally growing modes by Butler and Farrell,[15] of instantaneous turbulent flows by Hamilton *et al.*[3] and of weakly forced states by Coughlin.[20] However, our streamwise velocity u pictured in Fig. 13 differs significantly from Refs. 3 and 20 in that their u contours are much more strongly displaced at the vortex boundaries. This is

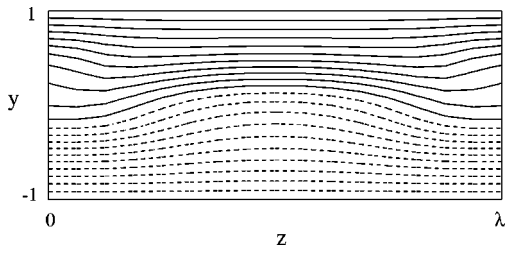

FIG. 13. Streamwise velocity contours in the plane $x=2$ for the 3-D field. Solid contours correspond to $u>0$, dashed contours to $u<0$.

probably due to the fact that our Reynolds number of 200 is substantially lower than their Re=400.

Far from the ribbon, the 3-D flow returns to plane Couette flow. Figure 14 compares the energy distribution $E(\mathbf{U}-\mathbf{U}_C)$ defined by (7) of the deviation of the 3-D flow from plane Couette flow at Re=200 with that at Re=250. Note that the 3-D flow is less localized than the corresponding eigenvector (Fig. 10). It can be seen that at the higher Reynolds number the deviation has higher energy, and importantly, occupies a larger streamwise extent. This is in accord with the experimental observation that the streamwise extent of vortices in the perturbed flow increases with increasing Reynolds number.

We have attempted to determine the location of the saddle-node bifurcation marking the lower Reynolds number limit of this branch of steady 3-D states; we believe that it occurs just below Re=200. There remains nevertheless a slight uncertainty regarding the lower bound for these states because we have found evidence of two different types of branches of steady 3-D states over the range $200 \leqslant \mathrm{Re} \leqslant 250$. The study of these states is further complicated by the fact that the time evolution to many of them is oscillatory, indicating that their least stable eigenvalues are a complex conjugate pair. Further investigation is required to ascertain the full nonlinear bifurcation diagram.

We have also sought to determine how the scenario changes as the ribbon radius ρ is decreased. Recall from Sec. III B that for $\rho=0.043$, we found $\mathrm{Re}_c \approx 550$. At these parameter values, 3-D simulations display chaotic time evolution.

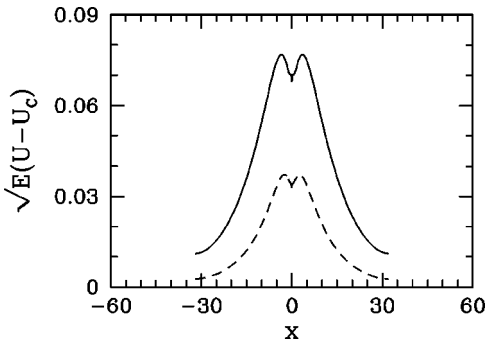

FIG. 14. Energy of deviation from plane Couette flow of 3-D velocity fields at Re=200 (dashed) and Re=250 (solid) as a function of x. The range in x is taken larger than the computational domain ($L=32$) to match the range of Figs. 5 and 10.

By decreasing Re, we have succeeded in computing a stable 3-D steady state at Re=350. Since the simulation showed chaotic oscillation for a long time (3000 time units) before showing signs of approaching a steady state, there remains the possibility that stable 3-D steady states are also attainable for higher Re. Simulations at Re=300 result in decay to the basic 2-D state (although we do not exclude the possibility of maintaining 3-D states by a more gradual decrease in Re). This is consistent with simulations of the unperturbed plane Couette geometry ($\rho=0$) by Hamilton *et al.*,[3] who observed chaotic oscillation for $\mathrm{Re} \geqslant 400$ and plane Couette flow $\mathbf{U}_C = y\hat{\mathbf{x}}$ for Re=300. Other numerical[2] and experimental[4,5] investigations in the unperturbed plane Couette geometry also indicate a critical Reynolds number of 360–375 for transition to turbulence. We plan to investigate the ρ dependence of the steady 3-D states and their stability in a future publication.

IV. CONCLUSION

We have performed a computational linear and nonlinear stability analysis of perturbed plane Couette flow in order to understand experiments recently performed at Saclay,[6–8] and more generally, three-dimensional flows in the plane Couette system. We have accurately determined the extent to which the basic steady 2-D profile is modified by the presence of a small spanwise-oriented ribbon in the flow. We have determined that such a ribbon, comparable in size to the cylinders used in the Saclay experiments, is large enough to induce linear instability of the basic profile at Reynolds numbers of order a few hundred.

We elaborate further on how our analysis complements the Saclay results. An experimental diagram was obtained[7,8] for the Reynolds number range of existence of various types of flows: 2-D, 3-D with streamwise vortices, intermittent, and turbulent. In these experiments it was not determined whether the 3-D streamwise vortices arise from a linear instability of the 2-D flow. Our results show that a small geometric perturbation does destabilize the 2-D flow in a subcritical instability and that the bifurcating solution is a 3-D flow with streamwise vortices. Specifically, for a nondimensional radius $\rho=0.086$, we find $\mathrm{Re}_c=230$ and for $\rho=0.043$, we find $\mathrm{Re}_c=550$. The computed spanwise wavelength of the most unstable mode is in good agreement with the value seen experimentally. The streamwise extent occupied by these vortices decreases with decreasing Reynolds number, as observed in experiment, and is finite at the lower Reynolds limit of the 3-D flows.

The Reynolds number ranges for the steady 3-D flows we have computed differ somewhat from those seen experimentally. For $\rho=0.086$, streamwise vortices were observed experimentally over the range $150 \lesssim \mathrm{Re} \lesssim 290$. For $\rho=0.086$, we have thus far found steady 3-D flows only if $\mathrm{Re} \geqslant 200$. In experiments with $\rho=0.043$, streamwise vortices have been observed over the range $190 \lesssim \mathrm{Re} \lesssim 310$; we have thus far found steady 3-D flows only for Re near 350. However, a full study of the 3-D flows is still pending and may resolve these discrepancies.

There are also minor qualitative differences between our results and the experimental findings. The first is that 2-D flows in our computations are more nearly antisymmetric in the cross-channel direction y than in experiment (our Fig. 4 vs Fig. 4 of Ref. 8). This is probably due to the fact that we perturb our flow with an infinitely thin ribbon and not a wire (cylinder) as in the experiment. However, based on the existence of instability in both cases, this small difference in the basic 2-D flow is probably not very significant. The other difference is due to the fact that our 3-D simulations impose spanwise periodicity with a single critical wavelength λ_c. Experimentally, it is observed that the streamwise vortices are not always regularly spaced in the spanwise direction.

As stated in Sec. I, streamwise vortices can be made to appear in channel flows via a number of approaches. Butler and Farrell[15] and Reddy and Henningson[16] show that under linear evolution, modes of this type can achieve very high amplitude before eventually being damped. In the pseudospectrum interpretation of Trefethen *et al.*,[17,16] nonnormality leads to sensitivity of the spectrum: streamwise vortices are unstable modes of a slightly perturbed linear stability matrix. Our results are entirely consistent with this interpretation: the ribbon or wire serves as a specific realization of a perturbation to the stability matrix, and has indeed rendered the flow linearly unstable to streamwise vortices.

Future computational work is needed to explore these flows. Calculating complete bifurcation diagrams for the two cases $\rho=0.086$ and $\rho=0.043$ is the first priority. We plan to study quantitatively and qualitatively the bifurcations at which the steady 3-D flows terminate at low Re and lose stability at high Re. Our goal is to continue 2-D and 3-D solutions of the perturbed system to the plane Couette case, $\rho=0$.

ACKNOWLEDGMENTS

This research was in part conducted while the authors were visitors at the Institute for Mathematics and its Applications (IMA) of the University of Minnesota, which is supported by the National Science Foundation. Some of the results were obtained using the supercomputer facilities of the Institut du Développement et des Ressources en Informatique Scientifique (IDRIS). We thank S. Bottin, A. Cherhabili, O. Dauchot, and K. Coughlin for discussing their results with us prior to publication. We also thank U. Ehrenstein, J. Guckenheimer, P. Manneville, M. Rossi, and L. N. Trefethen for interesting discussions. We gratefully acknowledge R. D. Henderson for the use of PRISM.

[1] B. J. Bayly, S. A. Orszag, and T. Herbert, ''Instability mechanisms in shear-flow transition,'' Annu. Rev. Fluid Mech. **20**, 359 (1988).
[2] A. Lundbladh and A. V. Johansson, ''Direct simulation of turbulent spots in plane Couette flow,'' J. Fluid Mech. **229**, 499 (1991).
[3] J. M. Hamilton, J. Kim, and F. Waleffe, ''Regeneration mechanisms of near-wall turbulence structures,'' J. Fluid Mech. **287**, 317 (1995).
[4] N. Tillmark and P. H. Alfredsson, ''Experiments on transition in plane Couette flow,'' J. Fluid Mech. **235**, 89 (1992).
[5] F. Daviaud, J. Hegseth, and P. Bergé, ''Subcritical transition to turbulence in plane Couette flow,'' Phys. Rev. Lett. **69**, 2511 (1992).
[6] O. Dauchot and F. Daviaud, ''Streamwise vortices in plane Couette flow,'' Phys. Fluids **7**, 901 (1995).
[7] S. Bottin, O. Dauchot, and F. Daviaud, ''Intermittency in a locally forced plane Couette flow,'' Phys. Rev. Lett. **79**, 4377 (1997).
[8] S. Bottin, O. Dauchot, F. Daviaud, and P. Manneville, ''Experimental evidence of streamwise vortices as finite amplitude solutions in transitional plane Couette flow,'' Phys. Fluids **10**, 2597 (1998).
[9] M. Nagata, ''Three-dimensional finite-amplitude solutions in plane Couette flow: Bifurcation from infinity,'' J. Fluid Mech. **217**, 519 (1990).
[10] M. Nagata, ''Tertiary solutions and their stability in rotating plane Couette flow,'' J. Fluid Mech. **358**, 357 (1998).
[11] A. J. Conley and H. B. Keller, ''Wavy Taylor vortices in plane Couette flow'' (unpublished).
[12] R. M. Clever and F. H. Busse, ''Three-dimensional convection in a horizontal fluid layer subjected to a constant shear,'' J. Fluid Mech. **234**, 511 (1992).
[13] A. Cherhabili and U. Ehrenstein, ''Spatially localized two-dimensional finite-amplitude states in plane Couette flow,'' Eur. J. Mech. B/Fluids **14**, 677 (1995).
[14] A. Cherhabili and U. Ehrenstein, ''Finite-amplitude equilibrium states in plane Couette flow,'' J. Fluid Mech. **342**, 159 (1997).
[15] K. M. Butler and B. F. Farrell, ''Three-dimensional optimal perturbations in viscous shear flow,'' Phys. Fluids A **4**, 1637 (1992).
[16] S. C. Reddy and D. S. Henningson, ''Energy growth in viscous channel flows,'' J. Fluid Mech. **252**, 209 (1993).
[17] L. N. Trefethen, A. E. Trefethen, S. C. Reddy, and T. A. Driscoll, ''Hydrodynamic stability without eigenvalues,'' Science **261**, 578 (1993).
[18] S. A. Orszag and L. C. Kells, ''Transition to turbulence in plane Poiseuille and plane Couette flow,'' J. Fluid Mech. **96**, 159 (1980).
[19] S. A. Orszag and A. T. Patera, ''Subcritical transition to turbulence in plane channel flows,'' Phys. Rev. Lett. **45**, 989 (1980).
[20] K. Coughlin, ''Coherent structures and intermittent turbulence in channel flows. 1. Coherent structures,'' submitted to J. Fluid Mech.
[21] M. Nishioka, S. Iida, and J. Ichikawa, ''An experimental investigation on the stability of plane Poiseuille flow,'' J. Fluid Mech. **72**, 731 (1975).
[22] M. F. Schatz, D. Barkley, and H. L. Swinney, ''Instability in a spatially periodic open flow,'' Phys. Fluids **7**, 344 (1995).
[23] A. T. Patera, ''A spectral element method for fluid dynamics; laminar flow in a channel expansion,'' J. Comput. Phys. **54**, 468 (1984).
[24] R. D. Henderson, ''Unstructured spectral element methods; parallel algorithms and simulations,'' Ph.D. thesis, Princeton University, 1994.
[25] R. D. Henderson and G. E. Karniadakis, ''Unstructured spectral element methods for simulation of turbulent flows,'' J. Comput. Phys. **122**, 191 (1995).
[26] G. E. Karniadakis, M. Israeli, and S. A. Orszag, ''High-order splitting methods for the incompressible Navier-Stokes equations,'' J. Comput. Phys. **97**, 414 (1991).
[27] D. Barkley and R. Henderson, ''Floquet stability analysis of the periodic wake of a circular cylinder,'' J. Fluid Mech. **322**, 215 (1996).
[28] R. D. Henderson and D. Barkley, ''Secondary instability in the wake of a circular cylinder,'' Phys. Fluids **8**, 1683 (1996).
[29] C. K. Mamun and L. S. Tuckerman, ''Asymmetry and Hopf bifurcation in spherical Couette flow,'' Phys. Fluids **7**, 80 (1995).